



Can stable isotopes ride out the storms? The role of convection for water isotopes in models, records, and paleoaltimetry studies in the central Andes



Alexander Rohrmann^{a,*}, Manfred R. Strecker^a, Bodo Bookhagen^{a,b}, Andreas Mulch^{c,d}, Dirk Sachse^{a,e}, Heiko Pingel^a, Ricardo N. Alonso^f, Taylor F. Schildgen^a, Carolina Montero^g

^a Institut für Erd- und Umweltwissenschaften, Universität Potsdam, 14476 Potsdam, Germany

^b Department of Geography, University of California, Santa Barbara, 93106 CA, USA

^c Biodiversity and Climate Research Centre (BiK-F) & Senckenberg, 60325 Frankfurt/Main, Germany

^d Institut für Geowissenschaften, Goethe Universität Frankfurt, 60438 Frankfurt/Main, Germany

^e GFZ German Research Centre for Geosciences, Section 5.1: Geoecology and Geomorphology, Telegrafenberg, 14473 Potsdam, Germany

^f Departamento de Geología, Universidad Nacional de Salta, CONICET, 4400 Salta, Argentina

^g Instituto de Bio y Geociencias del NOA (IBIGEO), Universidad Nacional de Salta, CONICET, 4400 Salta, Argentina

ARTICLE INFO

Article history:

Received 10 April 2014

Received in revised form 14 September 2014

Accepted 16 September 2014

Available online xxxx

Editor: G.M. Henderson

Keywords:

stable isotopes

Andes

precipitation

convection

paleoaltimetry

TRMM satellite data

ABSTRACT

Globally, changes in stable isotope ratios of oxygen and hydrogen ($\delta^{18}\text{O}$ and δD) in the meteoric water cycle result from distillation and evaporation processes. Isotope fractionation occurs when air masses rise in elevation, cool, and reduce their water-vapor holding capacity with decreasing temperature. As such, $\delta^{18}\text{O}$ and δD values from a variety of sedimentary archives are often used to reconstruct changes in continental paleohydrology as well as paleoaltimetry of mountain ranges. Based on 234 stream-water samples, we demonstrate that areas experiencing deep convective storms in the eastern south-central Andes (22–28° S) do not show the commonly observed relationship between $\delta^{18}\text{O}$ and δD with elevation. These convective storms arise from intermontane basins, where diurnal heating forces warm air masses upward, resulting in cloudbursts and raindrop evaporation. Especially at the boundary between the tropical and extra-tropical atmospheric circulation regimes where deep-convective storms are very common (~26° to 32° N and S), the impact of such storms may yield non-systematic stable isotope-elevation relationships as convection dominates over adiabatic lifting of air masses. Because convective storms can reduce or mask the depletion of heavy isotopes in precipitation as a function of elevation, linking modern or past topography to patterns of stable isotope proxy records can be compromised in mountainous regions, and atmospheric circulation models attempting to predict stable isotope patterns must have sufficiently high spatial resolution to capture the fractionation dynamics of convective cells.

© 2014 Elsevier B.V. All rights reserved.

1. Introduction

The use of oxygen and hydrogen stable isotopes ($\delta^{18}\text{O}$ and δD) in the meteoric water cycle has become common practice when assessing the complex relationships among tectonics, climate, topography, atmospheric circulation, and evapotranspiration of the biosphere (e.g. Dansgaard, 1964; Gonfiantini et al., 2001; Bowen and Wilkinson, 2002; Cerling et al., 1993; Dettman et al., 2003; Garzzone et al., 2008; Mix et al., 2013). Despite the plethora of applications of these isotopes as proxies for earth surface and atmospheric processes, there is still a lack of understanding of the

key factors that affect isotope distillation in orographic rainfall (Rozanski et al., 1993; Worden et al., 2007). This problem is especially relevant in high-elevation mountain ranges and plateau regions, where a systematic decrease in $\delta^{18}\text{O}$ and δD of meteoric waters with elevation is not observed, even though large temperature gradients as a function of elevation exist (Poage and Chamberlain, 2001; Rowley et al., 2001; Hren et al., 2009; Lechler and Niemi, 2012; Schemmel et al., 2013). Explanations for this phenomenon have included mixing of different moisture sources (Hren et al., 2009), high-elevation evaporation (Schemmel et al., 2013), and snow sublimation (Lechler and Niemi, 2012). Beyond these factors that likely contribute to discrepancies between expected/modeled and observed $\delta^{18}\text{O}$ and δD patterns in the geologic proxy record, the isotope-enabled atmospheric circulation

* Corresponding author.

E-mail address: rohrmann@geo.uni-potsdam.de (A. Rohrmann).

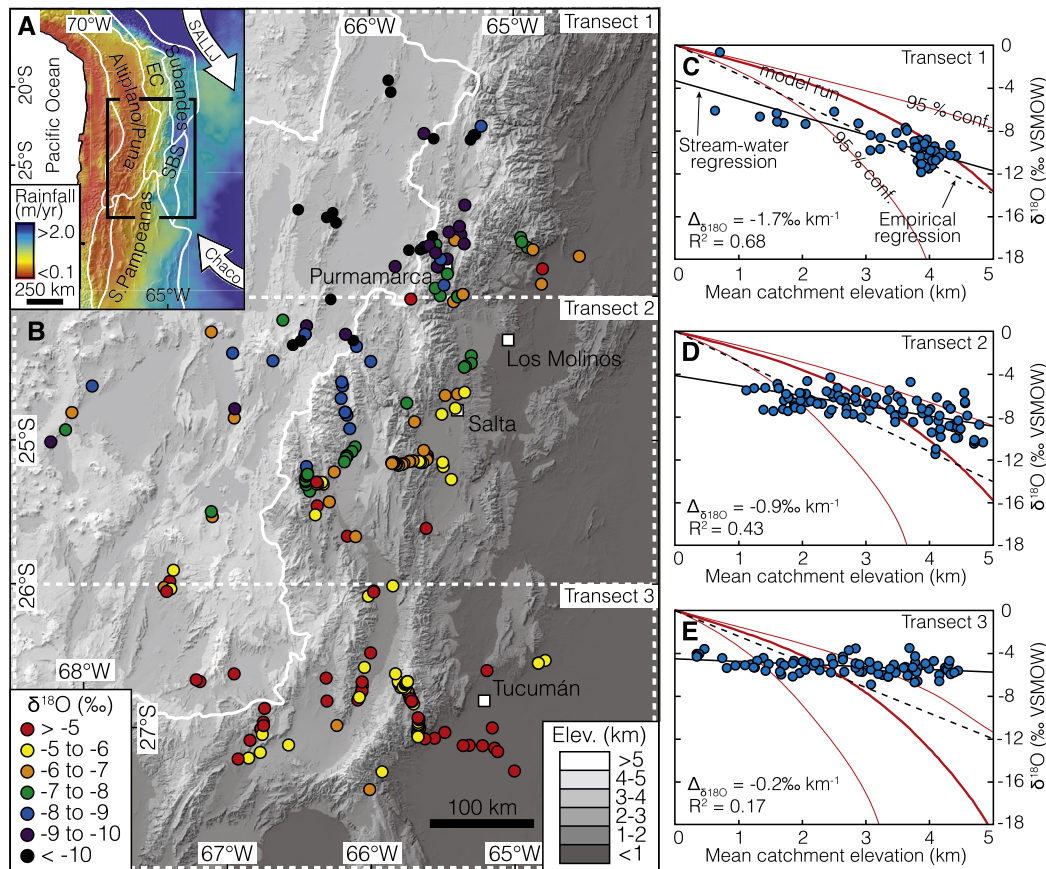


Fig. 1. Topography, rainfall, and stream-water $\delta^{18}\text{O}$ data for the south-central Andes. A. TRMM 3B42 annual rainfall and morphotectonic provinces (SBS: Santa Barbara System). Arrows highlight moisture transport (SALLJ – South American Low Level Jet) (Vera et al., 2006) and orogenward-moisture transport controlled by the Chaco low (Vuille et al., 2003). GNIP-stations from Fig. 2 are represented by white squares. B. SRTM DEM and stream-water color-coded $\delta^{18}\text{O}$ values (VSMOW). Right diagrams (C–E) represent mean-catchment elevation versus $\delta^{18}\text{O}$ (blue circles represent catchment samples), linear regression (solid black line) and global empirical fractionation curve (-2.8‰ km^{-1} , black dashed line) for each transect. Rowley et al. (2001) thermodynamic atmospheric model simulations based on DJF MOD11C2 night-temperature and NCEP-NCAR 1000 mbar re-analysis relative humidity data (%) from 2008 to 2013 (Kalnay et al., 1996) as starting model input parameters are shown in red.

and climate models themselves suffer from limitations that are attributed to (1) the low spatial resolution of General Circulation Models (>50 km), in which mesoscale circulation patterns, e.g., convective storms, cannot be reproduced and local topography is smoothed; (2) oversimplifications in models that tie temperature-dependent isotope fractionation directly to surface elevation; and (3) the low density of meteorological stations in arid and/or high-elevation terrains, which results in over-representation of station data from humid lowlands and valleys. Here, in a combined empirical and modeling approach, we investigate the effects of topographic relief, storminess, rainfall mode, moisture recycling, and airflow patterns on modern $\delta^{18}\text{O}$ and δD patterns in stream waters sampled along three E–W transects across eastern margin of the south-central Andes between ~ 22 and 28° S (Fig. 1) to unravel the relationships between $\delta^{18}\text{O}$ and δD values and storminess.

1.1. Precipitation and wind patterns along the south-central Andes

Extending from $\sim 7^\circ$ N to 45° S, with elevations rising to over 6 km, the Andes constitute a major orographic barrier to southern-hemisphere atmospheric circulation, exerting fundamental control on wind and precipitation patterns (Figs. 1a, 2 and Figs. S1, S2). For at least the last 7 to 8 Myr, the Andes have deflected moisture-bearing trade winds from the equatorial Atlantic and Amazonia towards the south to form the South American Low-Level Jet (SALLJ, Fig. 1a) (Vera et al., 2006; Uba et al., 2007; Mulch et al., 2010), which transports moisture to the eastern Andean flanks and accounts for annual rainfall of up to 3 m/yr

(Fig. 1a) (Bookhagen and Strecker, 2008). High seasonality results in $>80\%$ of the annual precipitation falling during the austral summer (December to February; Fig. 2) (Prohaska, 1976). To the south of the region affected by the SALLJ, a secondary jet (Chaco Jet) controlled by the Chaco Low influences moisture transport for the south-central Andes (Fig. 1a) (Salio et al., 2002; Saulo et al., 2004). The Chaco low forms in response to continental heating of the Andean foreland (Chaco plains) in northern Argentina and Paraguay (Salio et al., 2002). To the west, above the ca. 4-km high Altiplano–Puna plateau, a dry and stable westerly atmospheric airflow occurs at >500 mbar (>5 km; Figs. S1 and S2) (Garreaud et al., 2003). After crossing the plateau, the air descends along the eastern Andean flanks forming an orographic wave (Romatschke and Houze, 2013). To the east of the plateau, generally north–south oriented intermontane basins of the Eastern Cordillera and northern Sierras Pampeanas extend over areas of up to $\sim 10^4$ km². These basins are often bounded by ranges with topographic relief in excess of 3 km, rendering them very favorable to high nocturnal heat storage. The descent of upper atmospheric dry and stable air crossing the plateau prohibits orographic ascent of heated and moist air from the foreland and the plateau-parallel intermontane basins (Fig. 3 and Figs. S1 and S2). As a result of the different air-mass properties, an inversion develops. In such a scenario, rainfall is only produced by deep convective storms, which allow warm and humid air below the inversion to break through the overlying lid (Fig. 3b) (Zipser et al., 2006; Romatschke and Houze, 2013).

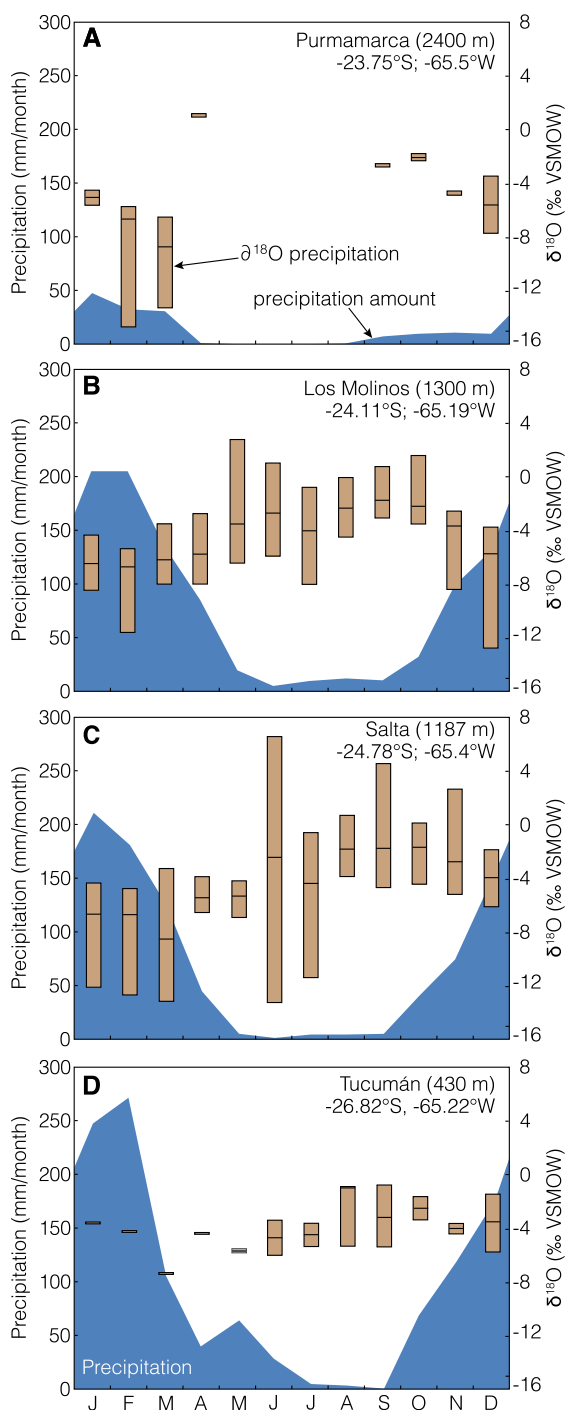


Fig. 2. Oxygen stable isotope and precipitation data for the GNIP-station from Tucumán, Salta, Los Molinos, and Purmamarca (IAEA, April 2012) (cf. Fig. 1). Brown boxes show oxygen stable isotope data in precipitation and blue boxes represents the mean monthly rainfall data. Tucumán station data represents 2 yrs of data from 01/05/2001 until 12/01/2002, Salta represents 22 yrs of data from 01/15/1981 to 12/15/2002, Los Molinos 9 yrs of data from 01/01/1981 to 12/01/1989 and Purmamarca 3 yrs of data from 01/01/1998 to 04/01/2000. Data are taken from the global IAEA/WMO website of Global Network of Isotopes in Precipitation. The GNIP Database is accessible at: <http://www.iaea.org/water> (IAEA, April 2012). (For color references in this figure legend, the reader is referred to the web version of this article.)

2. Methods

We established an extensive dataset of $\delta^{18}\text{O}$ and δD values of stream-water samples across the eastern border of the NW-Argentine Andes between ca. 22°S and 28°S . Our stream-water

sampling strategy included individual catchments along the eastern Andean flanks and the internally drained interior of the Puna plateau with upstream areas between 10 and 100 km^2 and contained flowing water. Field campaigns took place during the months of October through March from 2010 to 2013 with a sampling focus during December, January and February (DJF; Fig. 2; Table S1). As more than 80% of the mean annual rainfall occurs during DJF contrasted with generally dry austral winter (JJA) months (Fig. 2), we were able to capture the bulk of the annual signal of stream-waters. Samples were collected in 10 ml centrifuge tubes, sealed with plastic caps, and wrapped with parafilm and PTFE tape to prevent sample loss and evaporation prior to analysis. The elevation of each sampling location was recorded and catchment mean elevations were calculated using standard GIS methods. Mean catchment elevations range from 340 m in the east to 4836 m in the west, with high peak elevations well represented in all three transects.

Samples were analyzed at the joint Goethe University-BiK-F Stable Isotope facility at Goethe University Frankfurt. Stable hydrogen and oxygen isotope ratio measurements were made on 1 ml aliquots using an LGR 24d liquid isotope water analyzer. δD and $\delta^{18}\text{O}$ values were corrected based on internal laboratory standards calibrated against VSMOW (Vienna Standard Mean Ocean Water). The absolute analytical precision was typically better than 0.6‰ and 0.2‰ (both 2σ) for δD and $\delta^{18}\text{O}$, respectively. Absolute stable isotope values of the sample set range from -24 to -96 ‰ for δD and -4.5 to -13.0 ‰ for $\delta^{18}\text{O}$. Detailed results for all samples are presented in Table S1.

3. Results

To characterize the spatial distribution of $\delta^{18}\text{O}$ and δD in meteoric water (reported in VSMOW), we sampled 234 streams, lakes, springs, snow, and rainfall events over a period of four years along three E–W transects (Figs. 1b, 4a and Fig. S3; Table S1). All transects have the same easterly moisture source, but differ in topography, with relatively small intermontane basins and a distinct plateau margin in the north transitioning to large intermontane basins and a highly irregular plateau margin in the south (Figs. 1, 5 and Fig. S1). $\delta^{18}\text{O}$ values from stream waters range from -0.6 to -11.5 ‰ along transect 1 (22 to 24°S), -4.3 to -11.4 ‰ along transect 2 (between 24 to 26°S), and -2.3 to -6.9 ‰ along transect 3 (26 to 28°S ; Figs. 1 and 5). As we focus on studying the relationships of $\delta^{18}\text{O}$ and δD stream water with elevation, we define isotope lapse rates, $\Delta(\delta^{18}\text{O})$ and $\Delta(\delta\text{D})$, which reflect the change of $\delta^{18}\text{O}$ (or δD) as a function of elevation. A significant negative correlation between $\delta^{18}\text{O}$ and elevation exists in transect 1 with $\Delta(\delta^{18}\text{O}) = -1.7$ ‰ km^{-1} ($R^2 = 0.68$). Along transect 2, $\Delta(\delta^{18}\text{O})$ is reduced to -0.9 ‰ km^{-1} ($R^2 = 0.43$), while there is no significant relationship between elevation and $\delta^{18}\text{O}$ for transect 3 ($\Delta(\delta^{18}\text{O}) = -0.2$ ‰ km^{-1} with $R^2 = 0.17$). Each transect deviates from the global empirical relationship between $\delta^{18}\text{O}$ and elevation ($\Delta(\delta^{18}\text{O}) = -2.8$ ‰ km^{-1} ; Fig. 1), although deviations are much larger in the south (transect 3) compared to the north (transect 1) (Poage and Chamberlain, 2001). In general, there is an increase from -0.2 to -2.4 ‰ km^{-1} in the isotopic lapse rate from 28°S to 15°S along the eastern Andes when the data are compared to stable isotope stream-water data from Bolivia (Gonfiantini et al., 2001). South of 28°S , it is difficult to obtain data as aridity limits perennial stream flow. Stream-water data from a study near Mendoza ca 33°S indicate an isotopic lapse rate of up to -3.9 ‰ km^{-1} ; however, sample elevations below 2 km are strongly underrepresented and a spill-over effect of Pacific moisture has been reported there, complicating the comparison with our data from NW Argentina (Hoke et al., 2013).

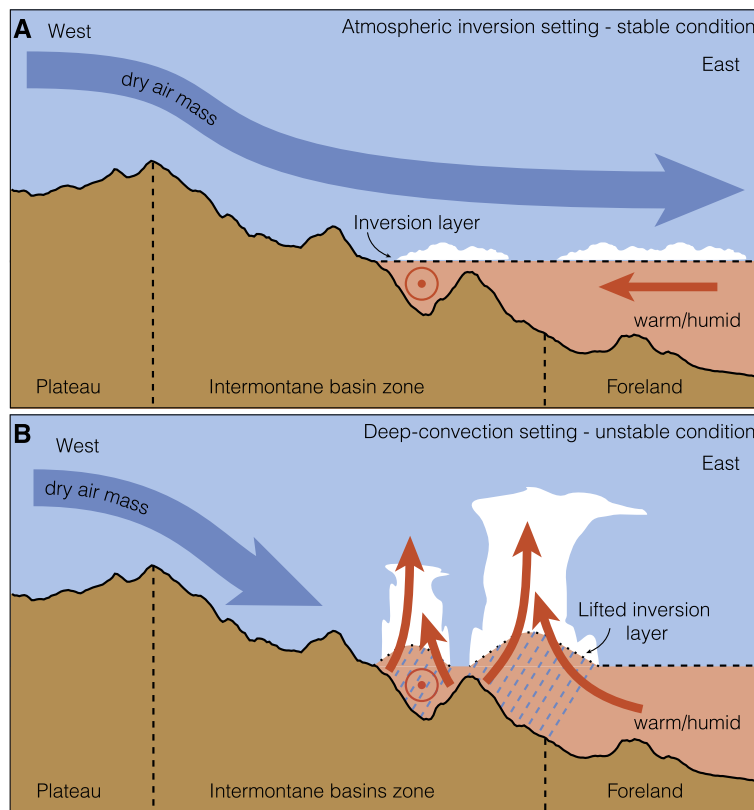


Fig. 3. Conceptual framework of the orographic wave, inversion (“capping”) and lifting (“triggering”) across the eastern Andean plateau margin. A: Inversion in place showing intact cap/boundary layer (heavy dashed line) between dry and adiabatically heated sinking air above and advected warm humid air below. B: Reduced orographic airflow and lifting of inversion (light dashed line) with strong upward lifting of warm humid air and eruption of deep-convective storms. Warm humid air in the intermontane basins below the inversion is connected with the foreland through topographic lows (river valleys), which help to advect the humid air mass into the interior (indicated by red circles with point). The large basins south of 24° S act as reservoirs for potential energy (resulting from daily solar heating) from which deep-convective storms can erupt.

4. Interpretations

4.1. Spatial patterns in oxygen and hydrogen stable isotope composition

Although all low-elevation foreland locations have similar $\delta^{18}\text{O}$ values of $\sim -4\text{‰}$ (Global Network of Isotopes in Precipitation (GNIP) stations; Fig. 2), our data show a strong north–south gradient in $\delta^{18}\text{O}$, isotopic lapse rate, and deuterium excess for the higher-elevation regions (Figs. 1b, 4b–c and 5) (IAEA/WMO, 2012). Deuterium excess (defined as $d = \delta\text{D} - 8 * \delta^{18}\text{O}$) is a parameter determined by non-equilibrium fractionation indicative of sub-cloud evaporation, moisture recycling, snow sublimation, or changes in moisture source (Stewart, 1975; Froehlich et al., 2008; Lechler and Niemi, 2012).

The large decrease in $\delta^{18}\text{O}$ ($< -10\text{‰}$) along transect 1 (northern transect) compared with $\delta^{18}\text{O}$ water values in the foreland is – to a first-order – similar to Rayleigh fractionation. Rayleigh distillation treats the isotopic composition as an open-system distillation, where precipitation is successively removed from the vapor as it condenses and the residual vapor is consistently depleted in ^{18}O and D (Dansgaard, 1964). This process is reflected in the good correlation of $\delta^{18}\text{O}$ with elevation (Figs. 1b and 5). The westward decrease in d from ca. 19‰ to -13‰ in transect 1 on the plateau is expected for ascending easterly humid air masses that progressively rainout above increasingly drier air. During rainout, sub-cloud evaporation of the falling rain droplets occurs, lowering the deuterium excess values (Fig. 5) (Stewart, 1975; Froehlich et al., 2008).

Along transect 2, the relationship between $\delta^{18}\text{O}$ and elevation weakens, and it essentially disappears along transect 3. There, $\delta^{18}\text{O}$

and deuterium excess values from the foreland to the plateau margin are virtually constant (Figs. 1b and 5). Such a pattern is inconsistent with simple orographic lifting of warm, humid air masses and associated rainout. Rather, it is indicative of upward convective mixing, resulting in limited open-system distillation necessary for Rayleigh fractionation and hence limited oxygen (and hydrogen) isotope fractionation of precipitation falling at the Earth’s surface. Across the entire latitudinal swath from 22° to 28° S, a strong $\delta^{18}\text{O}$ gradient is prominent (Figs. 1 and 4b–c). Moreover, there are systematic relationships of the $\delta^{18}\text{O}$ values at different elevation intervals as the gradient in the amount of ^{18}O depletion (and hence the isotopic lapse rate) increases with elevation from south to north (Fig. 4b–c). This trend suggests that convection is not only limited to the southernmost transect, but also that the amount of convective rainfall decreases northward, thus directly affecting the observed oxygen-isotope lapse rates (Fig. 1). D-excess (d) shows no trend with latitude, illustrating that the moisture source along all three transects is similar and derived from the Amazon Basin (Figs. 1 and 4b–c). However, several samples at elevations > 4 km show much more negative d values, likely resulting from mixing with a Pacific moisture source.

4.2. Temperature-lapse rates and modeling of stable isotopes in precipitation

To gain additional insight into the controls on $\delta^{18}\text{O}$ and δD values of meteoric water in the Central Andes, we use a numerical thermodynamic Rayleigh condensation model to predict stable isotopic compositions along the sampled transects (Fig. 1b; and Supplementary materials for further details)

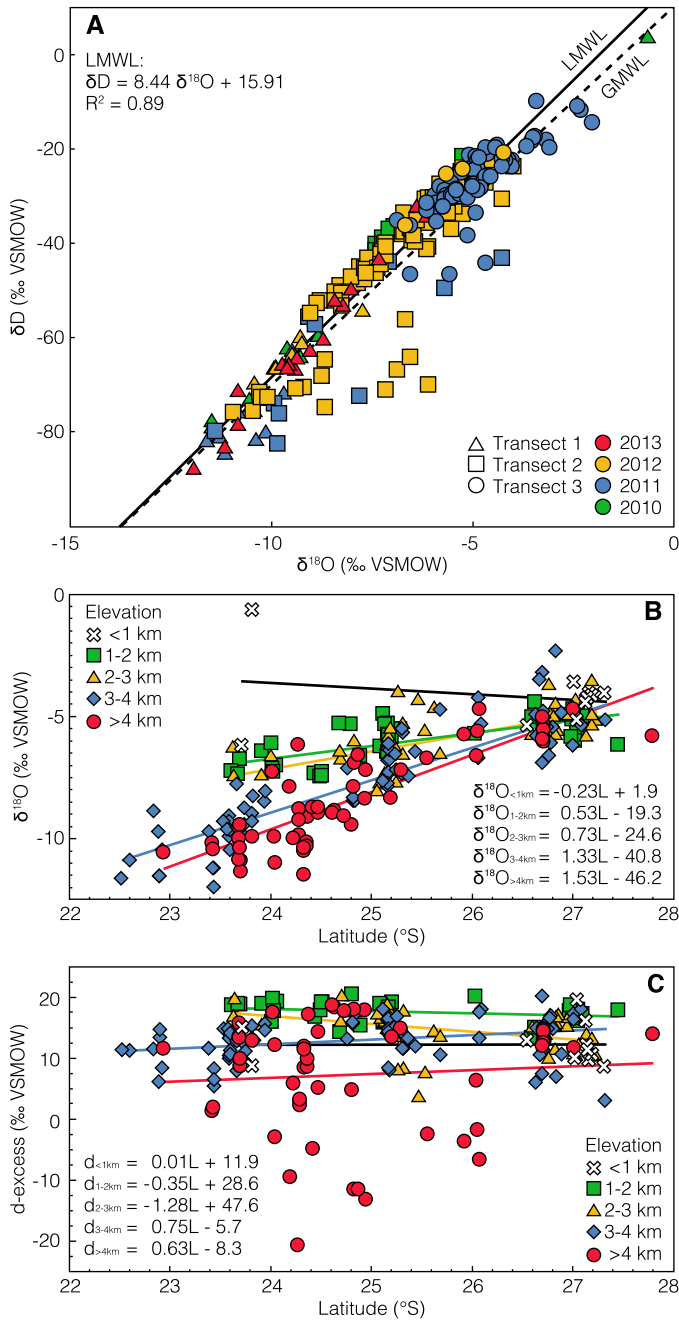


Fig. 4. Stream-water $\delta^{18}O$, δD , and D-excess data and latitudinal distribution. A. $\delta^{18}O$ versus δD values shape-coded for different water transects and color-coded for their sampling year. Dashed black line represents the global meteoric water line (GMWL) and solid black line is the local meteoric water line (LMWL). B. $\delta^{18}O$ values of stream-water data against latitude. Symbol-color coded objects represent 1-km bins and illustrate the large latitudinal gradient in stream-water. C. 1-km binned D-excess values of stream water data with latitude. Note the scatter in data from elevations >4 km potentially showing Pacific moisture mixing.

(Rowley et al., 2001). First, we define a surface temperature-lapse rate for each transect based on 12 yrs of satellite-derived DJF land-surface temperature data (MOD11C2) to obtain input starting temperatures for the model (Figs. 6a and 7; and Supplementary materials for further details) (Wan et al., 2002). The MODIS satellite data are calibrated against surface stations and have accuracies of better than 1°C (Wan, 2008). In general, temperature-lapse rates below 2000 m are in line with a dry adiabatic cooling trend of $\sim 1.0^\circ\text{C}$ per 100 m, whereas at eleva-

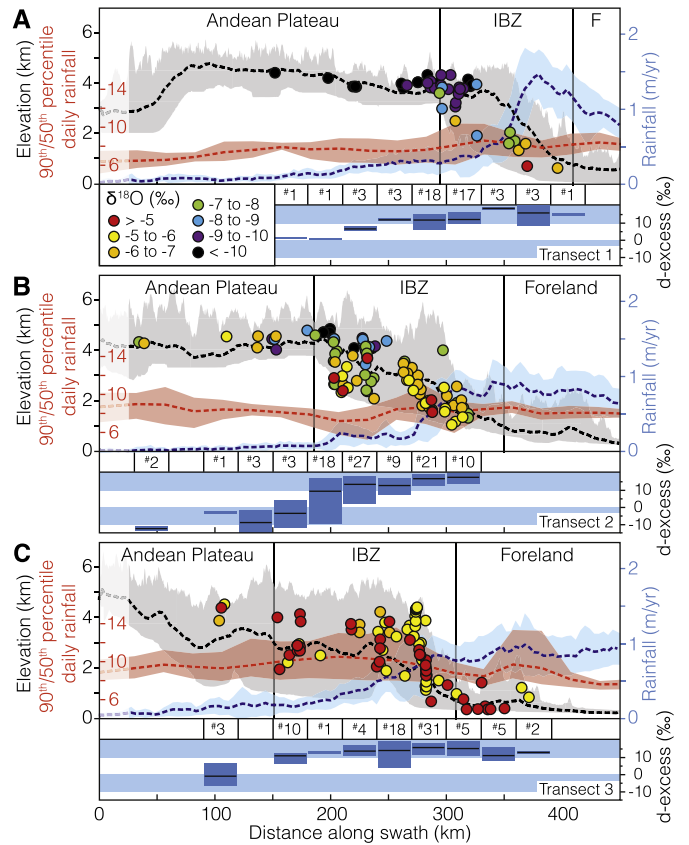


Fig. 5. Swath profiles showing maximum, minimum (gray shading), and mean elevation (black) TRMM-2B31 rainfall data (blue) (Bookhagen and Strecker, 2008), and TRMM 3B42 V7 90th/50th percentile ratio of daily rainfall (red) across the south-central Andes outlined in Fig. 1 (Huffman et al., 2007; Boers et al., 2013). Stable isotopic values ($\delta^{18}O$) have the same color scale as in Fig. 1. Blue bins below each transect show range and mean (gray line) of deuterium excess values along the profile. Each box represents samples located in a 30-km-wide interval with numbers of samples for each bin shown above.

tions above 2000 m, they follow a moist-adiabatic cooling trend of 0.5°C per 100 m (Fig. 7). Consequently, the obtained data set was subdivided into elevations above and below 2000 m based on the different temperature lapse-rate trends. For transect 1, lapse rates <2000 m are $-0.92^\circ\text{C}/100\text{ m}$ ($n = 134$, $R^2 = 0.85$, $p \ll 0.01$) and $-0.21^\circ\text{C}/100\text{ m}$ for >2000 m ($n = 855$, $R^2 = 0.63$, $p \ll 0.01$); transect 2 lapse rates <2000 m are $-0.80^\circ\text{C}/100\text{ m}$ ($n = 346$, $R^2 = 0.55$, $p \ll 0.01$) and $-0.38^\circ\text{C}/100\text{ m}$ for >2000 m ($n = 1965$, $R^2 = 0.63$, $p \ll 0.01$); transect 3 lapse rates <2000 m are $-0.64^\circ\text{C}/100\text{ m}$ ($n = 748$, $R^2 = 0.74$, $p \ll 0.01$) and $-0.47^\circ\text{C}/100\text{ m}$ for >2000 m ($n = 2121$, $R^2 = 0.68$, $p \ll 0.01$) (Fig. 7). The null hypothesis for the p -values was that the elevation (x) and temperature (y) are derived from independent, random samples from normal distributions with equal means and equal, but unknown variances. For the model input humidity starting parameters, we used the NCEP–NCAR 1000 mbar re-analysis relative humidity data (%) from 2008 to 2013 (Kalnay et al., 1996).

The thermodynamic Rayleigh condensation model based on atmospheric temperature-lapse rates and fractionation with elevation as rising air masses cool provides a reasonable prediction of observed isotopic compositions along transect 1 (red lines; Fig. 1c–e). Isotope $\delta^{18}O$ values >3 km are well represented, whereas lower elevations show a mismatch between observed and modeled values, likely due to downstream mixing of higher-elevation stream water. However, in transect 2, the fit of predicted $\delta^{18}O$ and δD values weakens, as high-elevation samples obtained in locations >4 km start to fall outside the model’s 95% confidence

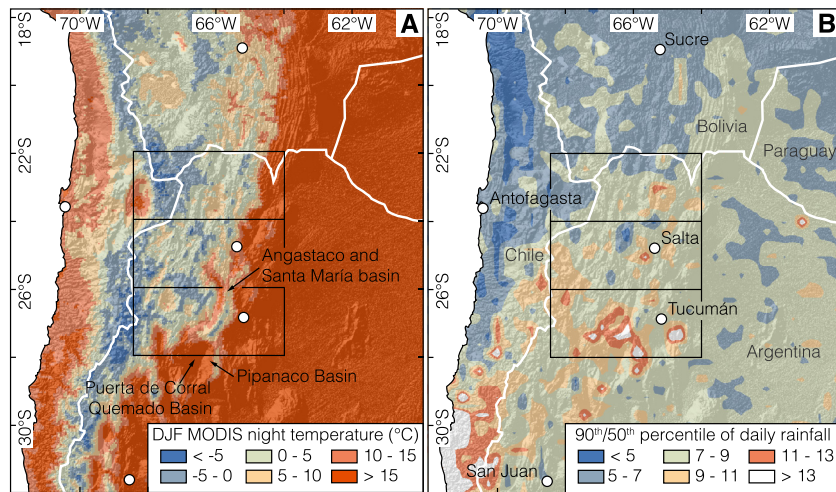


Fig. 6. A. TRMM-3B42 V7 90th/50th percentile of daily rainfall data averaged over 15 yrs (Huffman et al., 2007; Boers et al., 2013). Low ratios indicate a narrow rainfall distribution (i.e., stratiform rainfall), whereas high ratios indicate a 'heavy-tail' rainfall distribution (i.e., deep convective storms). White lines represent international borders. B. Night land surface temperatures (MOD11C2) (Wan et al., 2002) for DJF averaged over 12 yrs. Note the intermontane basins between 26° and 30° S storing excess heat and potential energy for convection.

level. In transect 3, the model does not match the observed $\delta^{18}\text{O}$ pattern at all. Especially, elevations > 3 km plot outside the model bounds, implying that fractionation here does not follow open-system behavior, which is a prerequisite for Rayleigh fractionation (Fig. 1e).

4.3. Tracing convective rainfall and storminess

Similar to other plateau margins worldwide, strong insolation, high humidity, and pronounced topographic and relief gradients along the windward flanks of the Andean plateau result in frequent and extreme hydro-meteorological events (Zipser et al., 2006; Bookhagen and Strecker, 2008; Romatschke and Houze, 2013). High-spatial resolution TRMM-2B31 and 2A25 satellite data (Tropical Rainfall Measuring Mission – TRMM) allows for examination of convection processes and precipitation patterns between 36° N and 36° S (Huffman et al., 2007; Bookhagen and Strecker, 2008; Romatschke and Houze, 2013). We use TRMM 3B42V7 90th/50th percentile ratios for daily rainfall as a proxy for deep-convective rainfall and to define patterns of strong convection and storminess (Huffman et al., 2007; Boers et al., 2013) (Fig. 6b). We normalize extreme rainfall amounts associated with convective storms (90th percentile) by the median (50th percentile) for each pixel to document distinct spatial patterns in rainfall extreme events (Fig. 6b). The 90th/50th percentile ratio is a measure of how skewed the rainfall distribution is for a particular area and thus cannot identify the mode of precipitation. Therefore, it is necessary to identify the source (e.g., convection) of the skewness in the rainfall data to interpret the 90th/50th percentile data accurately. For example, the high 90th/50th percentile ratios along the western flank of the Andes do not exhibit convective nature, but reflect very strong, infrequent wintertime frontal rainfall events producing a skewed rainfall distribution (Fig. 6b).

In the Eastern Andes, the high 90th/50th percentile ratios south of 26° S (Fig. 6b) agree well with TRMM-Precipitation Radar data (PR, product 2A25), which characterizes the nature of rainfall in South America and also shows frequent deep-convective storms south of 26° S (Romatschke and Houze, 2013). There, the trigger for convection is not diurnal heating as elsewhere in the tropics, but rather conditions favorable to lifting the inversion found along the south-central Andes over intermontane basins (Fig. 3 and Fig. S4) (Romatschke and Houze, 2013). Specifically, daytime warming of large intermontane basins stores significant potential

heat, which is available at night to lift the inversion and promote deep-convective storms (Fig. 6a). The rapid lifting of warm, humid air from beneath the inversion causes rapid upward convective mixing of moisture, resulting in limited open system distillation. As a result, convective rainfall does not systematically deplete the air mass of heavy isotopes, because moisture recycling replenishes the depleted air at high elevation (Risi et al., 2008). Hence, convective air circulation allows storms to cross high topography without major depletion in ^{18}O or D, as illustrated by consistently high deuterium-excess values along transect 3 and only slightly decreasing deuterium-excess values in transect 2 (Figs. 4 and 5).

5. Discussion

5.1. Controls on stable-isotope systematics

Our results demonstrate that despite general agreement with globally observed stable isotope-elevation relationships in transect 1, elevation does not exert a first-order control on $\delta^{18}\text{O}$ values in the southernmost transects across the southern-central Andes (Figs. 1, 4 and 5). This interpretation is supported by the virtual absence of a relationship between rainfall amount and topographic relief (Fig. 5). In contrast, $\delta^{18}\text{O}$ and δD stream-water samples along transect 1 agree with other available studies of $\delta^{18}\text{O}$ and δD located north of 22° S, where the climate is generally more humid and the tropical atmosphere regime is characterized by lower storm frequencies (Fig. 6b) (Confiantini et al., 2001; Insel et al., 2012). In the region of transect 1, the temperature-lapse rate with elevation drives rainout and stable-isotope fractionation, but this is not the case south of 26° S along transect 3, which is influenced by the extra-tropical atmospheric circulation regime and increased convection (Fig. 5). These contrasting patterns in our data between the northern and southern transects exemplify how studies of $\delta^{18}\text{O}$ and δD at the boundary between the tropics and extra-tropics ($\sim 26^\circ$ to 32° N and S) can be strongly affected by deep convective storms (Fig. 6). Consequently, repeated convective storms may yield unexpected and non-systematic oxygen-isotope lapse rates as a function of elevation. In such cases, the assumption of temperature-controlled rainout with elevation producing a systematic isotopic lapse rate can be severely compromised. Our data are the first to demonstrate the causes and consequences of missing oxygen (and hydrogen) isotope depletion in the presence of large temperature gradients with elevation, and particularly how

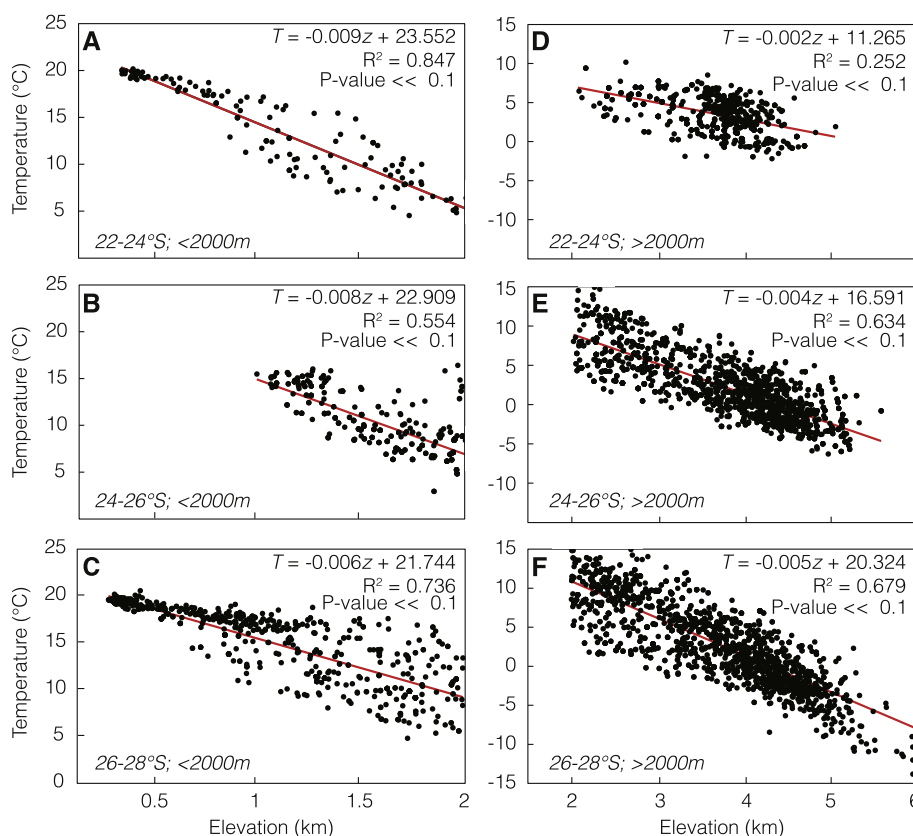


Fig. 7. MOD11C2 night land surface temperatures for December, January, and February (DJF) averaged over 12 yrs from 2000 to 2012. The temperature data are divided into elevations above and below 2 km. Raster resolution is 5.5 km and black points represent temperature information of individual cells. Only cells overlapping sampled catchments are used for calculating temperature-lapse rates. Note the differences between lapse rates above and below 2 km. Lapse rates below 2 km are much closer to dry adiabatic cooling trend, whereas above 2 km, a very suppressed wet adiabatic cooling trend is observed.

deep-convection can overprint isotope systematics in precipitation as upward moisture mixing in storms violates the open-system assumption in Rayleigh fractionation.

5.2. Implications for isotope-enabled atmospheric circulation models, paleoenvironmental studies, and paleoaltimetry studies

Reconstructions of paleo-environmental conditions and the topographic evolution of mountain belts are often derived from stable isotope proxies in materials such as pedogenic carbonates, volcanic glass, mammal-tooth enamel, or organic compounds. Each of these materials retains the $\delta^{18}\text{O}$ or δD composition of ancient meteoric waters (e.g. Lee-Thorpe and Van der Merwe, 1987; Cerling et al., 1993; Garzzone et al., 2008; Mulch et al., 2008; Sachse et al., 2012). Especially for materials that capture short-term variations in the isotopic composition of rainfall, the absence of systematic stable isotope-elevation relationships may render any paleoaltimetry interpretation complex, if not impossible (Blisniuk and Stern, 2005). Our results therefore have major implications for understanding, interpreting, and modeling present and past $\delta^{18}\text{O}$ and δD data, especially regarding paleoelevation and paleoenvironment assessments within and along the Andean orogeny and beyond.

First, current stable-isotope enabled General Circulation Models rely solely on adiabatic cooling and temperature fractionation induced by changes in elevation. Our results demonstrate the need for sufficiently high resolution in these models to capture regional mesoscale convective cells, which would far more accurately reflect regional stable isotope values of precipitation. Otherwise, modeled $\delta^{18}\text{O}$ and δD values will substantially deviate from observation data, a phenomenon observable for the region along our transect 3,

which is characterized by highly convective rainfall (Insel et al., 2012).

Second, in regions with deep convection, it will be difficult to reliably reconstruct topography or paleoenvironmental conditions through stable-isotope approaches, because strong convection may reduce or mask any elevation signal in the geologic proxy record. Therefore, interpretations of $\delta^{18}\text{O}$ and δD records (e.g., from pedogenic carbonates, lipid-biomarkers, or tooth enamel) that assume simple Rayleigh fractionation in areas influenced by deep convection at the tropical–extratropical boundary may provide misleading information on the elevation and/or climate history and should be validated against additional proxy records. As an example, $\delta^{18}\text{O}$ values from pedogenic carbonate and mammal teeth of Tertiary sediments within the deep-convective zone of transect 3 at 27.5° S/67° W (Fig. 1) at the Puerta de Corral Quemado intermontane basin show little variability (-7.5 to -4.5‰) between ~ 8 to 3 Ma (Latorre et al., 1997; Hynek et al., 2012). Nonetheless, several lines of evidence indicate a pronounced phase of mountain building and surface uplift during that time. At ~ 6 Ma, low-temperature thermochronology data derived from adjacent basement ranges and sediment characteristics of the adjacent basins indicate that ranges to the north and east of the basin were uplifted and started forming orographic barriers (Strecker et al., 1989; Bossi et al., 2001; Kleinert and Strecker, 2001; Sobel and Strecker, 2003). These range uplifts blocked moist easterly airflow and induced changes from C3 to C4 plant communities in the basin (Hynek et al., 2012). The lack of concurrent significant variation in the $\delta^{18}\text{O}$ record likely indicates that the region was influenced by convective storms, both between ~ 8 to 3 Ma as well as today.

In the context of these paleo-environmental studies, we caution that only those areas that are not affected by deep-convection

may be appropriate for stable isotope paleoaltimetry – an approach whose applicability and reliability has been intensely discussed over the past decade (e.g. Poage and Chamberlain, 2001; Blisniuk and Stern, 2005; Rowley and Garzzone, 2007; Ehlers and Poulsen, 2009). We also conclude that the complicating effects of convective rainfall have not been fully considered in a variety of stable isotope paleoaltimetry studies in the southern-central Andes (e.g. Canavan et al., 2014; Carrapa et al., 2014). This oversight may potentially lead to oversimplified misinterpretations of quasi-constant stable isotope – elevation relationships in regions that today (and likely in the past) were strongly subjected to convective rainfall conditions. Conversely, farther north, where extensive intermontane basins are less frequent and deep convective storms are typically not generated (e.g., regions adjacent to the Subandean fold-and-thrust belt or in the Eastern Cordillera), our identification of Rayleigh fractionation in modern precipitation is encouraging for stable isotope paleoaltimetry studies.

6. Conclusions

Overall, our results add a new element in the interpretation of stable isotope data from precipitation along elevation/temperature transects, particularly when attempting to interpret past records of $\delta^{18}\text{O}$ and δD . Such present-day validation studies of water stable-isotope patterns are crucial for extra-tropical regions that are affected by deep-convection, as convection can disrupt simple patterns of rainout and Rayleigh isotopic fractionation with increasing elevation. Understanding atmospheric circulation patterns along plateau margins with pronounced rainfall gradients, such as the Altiplano–Puna or Himalaya–Tibetan Plateau, is of particular importance, as strong convection cells can arise not only from areally extensive intermontane basins and foreland regions, but also from steep topographic barriers. In summary, our results illustrate that (1) atmospheric convection can strongly affect $\delta^{18}\text{O}$ and δD in precipitation and overprint simple relationships between stable isotopes in precipitation and elevation that are due to temperature-controlled fractionation and orographic lifting; (2) isotope-in-precipitation models based on temperature-related fractionation alone that do not have sufficient spatial resolution to capture convective storms can deviate substantially from the observed $\delta^{18}\text{O}$ and δD patterns; and (3) in regions with convective rainfall, we emphasize the necessity for careful assessments of modern $\delta^{18}\text{O}$ and δD data before attempting to interpret $\delta^{18}\text{O}$ and δD data in the geologic record.

Acknowledgements

This study was funded by Deutsche Forschungsgemeinschaft (DFG joint grants: STR 373/32-1, MU2845/4-1) with support from the DFG-Leibniz Center for Surface Processes and Climate Studies at Universität Potsdam, Germany (DFG 373/18-1) and the LOEWE funding program (Landes-Offensive zur Entwicklung wissenschaftlich-ökonomischer Exzellenz) of Hesse's Ministry of Higher Education, Research, and the Arts. D. Sachse was supported by a DFG Emmy-Noether grant (SA1889/1-1). We acknowledge the support of J. Fiebig at the Joint Goethe University – BiK-F stable isotope facility Frankfurt and H. Meyer at the Alfred-Wegener-Institute in Potsdam. We thank D. Rowley, M. Hren and an anonymous reviewer for insightful reviews.

Appendix A. Supplementary material

Supplementary material related to this article can be found online at <http://dx.doi.org/10.1016/j.epsl.2014.09.021>.

References

- Blisniuk, P.M., Stern, L.A., 2005. Stable isotope paleoaltimetry: a critical review. *Am. J. Sci.* 305, 1033–1074.
- Boers, N., Bookhagen, B., Marwan, N., Kurths, J., Marengo, J., 2013. Complex networks identify spatial patterns of extreme rainfall events of the South American Monsoon System. *Geophys. Res. Lett.* 40 (16), 4386–4392.
- Bookhagen, B., Strecker, M.R., 2008. Orographic barriers, high-resolution TRMM rainfall, and relief variations along the eastern Andes. *Geophys. Res. Lett.* 35 (6), 1–6.
- Bossi, G.E., Georgieff, S.M., Gavrilloff, I.J.C., Ibañez, L.M., Muruaga, C.M., 2001. Cenozoic evolution of the intramontane Santa Maria basin, Pampean Ranges, northwestern Argentina. *J. South Am. Earth Sci.* 14 (7), 725–734.
- Bowen, G.J., Wilkinson, B., 2002. Spatial distribution of $\delta^{18}\text{O}$ in meteoric precipitation. *Geology* 30, 315–318.
- Canavan, R.R., Carrapa, B., Clementz, M.T., Quade, J., DeCelles, P.G., Schoenbohm, L.M., 2014. Early Cenozoic uplift of the Puna Plateau, Central Andes, based on stable isotope paleoaltimetry of hydrated volcanic glass. *Geology*. <http://dx.doi.org/10.1130/G35239.1>.
- Carrapa, B., Huntington, K.W., Clementz, M., Quade, J., Bywater-Reyes, S., Schoenbohm, L.M., Canavan, R.R., 2014. Uplift of the Central Andes of NW Argentina associated with upper crustal shortening, revealed by multiproxy isotopic analyses. *Tectonics* 33 (6), 1039–1054. <http://dx.doi.org/10.1002/2013TC003461>.
- Cerling, T.E., Wang, Y., Quade, J., 1993. Expansion of C4 ecosystems as an indicator of global climatic change in the late Miocene. *Nature* 361, 344–345.
- Dansgaard, W., 1964. Stable isotopes in precipitation. *Tellus* 16 (4), 436–468.
- Dettman, D.L., Fang, X., Garzzone, C.N., Li, J., 2003. Uplift-driven climate change at 12 Ma: a long $\delta^{18}\text{O}$ record from the NE margin of the Tibetan plateau. *Earth Planet. Sci. Lett.* 2148 (1–2), 267–277.
- Ehlers, T.A., Poulsen, C.J., 2009. Influence of Andean uplift on climate and paleoaltimetry estimates. *Earth Planet. Sci. Lett.* 281 (3–4), 238–248.
- Froehlich, K., Kralik, M., Papesch, W., Scheifinger, H., Stichler, W., 2008. Deuterium excess in precipitation of Alpine regions – moisture recycling. *Isot. Environ. Health Stud.* 44 (1), 61–70.
- Garreaud, R., Vuille, M., Clement, A.C., 2003. The climate of the Altiplano: observed current conditions and mechanisms of past changes. *Palaeogeogr. Palaeoclimatol. Palaeoecol.* 194 (1–3), 5–22.
- Garzzone, C.N., et al., 2008. Rise of the Andes. *Science* 320 (5881), 1304–1307.
- Gonfiantini, R., Roche, M.A., Olivery, J.C., Fontes, J.C., Zuppi, G.M., 2001. The altitude effect on the isotopic composition of tropical rains. *Chem. Geol.* 181, 147–167.
- Hoke, G.D., Aranibar, J.N., Viale, M., Araneo, D.C., Llano, C., 2013. Seasonal moisture sources and the isotopic composition of precipitation, rivers, and carbonates across the Andes at 32.5–35.5° S. *Geochem. Geophys. Geosyst.* 14, 1–17. <http://dx.doi.org/10.1002/ggge.20045>.
- Hren, M.T., Bookhagen, B., Blisniuk, P.M., Booth, A.L., Chamberlain, C.P., 2009. $\delta^{18}\text{O}$ and δD of streamwaters across the Himalaya and Tibetan Plateau: implications for moisture sources and paleoelevation reconstructions. *Earth Planet. Sci. Lett.* 288 (1–2), 20–32.
- Huffman, G.J., et al., 2007. The TRMM multisatellite precipitation analysis (TMPA): quasi-global, multiyear, combined-sensor precipitation estimates at fine scales. *J. Hydrometeorol.* 8 (1), 38–55.
- Hynek, S., Passey, B.H., Prado, J.L., Brown, F.H., Cerling, T.E., Quade, J., 2012. Small mammal carbon isotope ecology across the Miocene–Pliocene boundary, northwestern Argentina. *Earth Planet. Sci. Lett.* 321–322, 177–188.
- IAEA/WMO, 2012. Global network of isotopes in precipitation, the GNIP database. Accessible at: <http://www.iaea.org/water>.
- Insel, N., Poulsen, C.J., Ehlers, T.A., Sturm, C., 2012. Response of meteoric $\delta^{18}\text{O}$ to surface uplift – implications for Cenozoic Andean Plateau growth. *Earth Planet. Sci. Lett.* 317–318, 262–272.
- Kalnay, E., et al., 1996. The NCEP/NCAR reanalysis 40-year project. *Bull. Am. Meteorol. Soc.* 77 (3), 437–471.
- Kleinert, K., Strecker, M.R., 2001. Climate change in response to orographic barrier uplift: paleosol and stable isotope evidence from the late Neogene Santa Maria basin, northwestern Argentina. *Geol. Soc. Am. Bull.* 113 (6), 728–742.
- Latorre, C., Quade, J., McIntosh, W.C., 1997. The expansion of C4 grasses and global change in the late Miocene: stable isotope evidence from the Americas. *Earth Planet. Sci. Lett.* 146, 83–96.
- Lechler, A.R., Niemi, N.A., 2012. The influence of snow sublimation on the isotopic composition of spring and surface waters in the southwestern United States: implications for stable isotope-based paleoaltimetry and hydrologic studies. *Geol. Soc. Am. Bull.* 124 (3–4), 318–334.
- Lee-Thorpe, J.L., Van der Merwe, N.J., 1987. Carbon isotope analysis of fossil bone apatite. *South Afr. J. Sci.* 83 (11), 712–715.
- Mix, H., Winnick, M.J., Mulch, A., Chamberlain, C.P., 2013. Grassland expansion as an instrument of hydrologic change in Neogene western North America. *Earth Planet. Sci. Lett.* 377–378, 73–83.

- Mulch, A., Sarna-Wojcicki, A.M., Perkins, M.E., Chamberlain, C.P., 2008. A Miocene to Pleistocene climate and elevation record of the Sierra Nevada (California). *Proc. Natl. Acad. Sci. USA* 105, 6819–6824.
- Mulch, A., Uba, C., Strecker, M.R., Schönberg, R., Chamberlain, C.P., 2010. Late Miocene climate variability and surface elevation in the central Andes. *Earth Planet. Sci. Lett.* 290, 173–182.
- Poage, M.A., Chamberlain, C.P., 2001. Stable isotope composition of precipitation and surface waters: considerations for studies of paleoelevation change. *Am. J. Sci.* 301 (1), 1–15.
- Prohaska, F., 1976. The climate of Argentina, Paraguay and Uruguay. In: *Climates of Central and South America*. In: *World Survey of Climatology*.
- Risi, C., Bony, S., Vimeux, F., 2008. Influence of convective processes on the isotopic composition ($\delta^{18}\text{O}$ and δD) of precipitation and water vapor in the tropics: 2. Physical interpretation of the amount effect. *J. Geophys. Res.* 113 (D19), 1–12.
- Romatschke, U., Houze, R., 2013. A characteristics of precipitating convective systems accounting for the summer rainfall of tropical and subtropical South America. *J. Hydrometeorol.* 14 (1), 25–46.
- Rowley, D.B., Garzione, C.N., 2007. Stable isotope-based paleoaltimetry. *Annu. Rev. Earth Planet. Sci.* 35 (1), 463–508.
- Rowley, D.B., Pierrehumbert, R.T., Currie, B.S., 2001. A new approach to stable isotope-based paleoaltimetry: implications for paleoaltimetry and paleohypsometry of the High Himalaya since the Late Miocene. *Earth Planet. Sci. Lett.* 188, 253–268. [http://dx.doi.org/10.1016/S0012-821X\(01\)00324-7](http://dx.doi.org/10.1016/S0012-821X(01)00324-7).
- Rozanski, K., Araguás-Araguás, L., Gonfiantini, R., 1993. Isotopic patterns in modern global precipitation, climate change in continental isotopic records. *Geophys. Monogr.* 78, 1–36.
- Sachse, D., et al., 2012. Molecular paleohydrology: interpreting the hydrogen-isotopic composition of lipid biomarkers from photosynthesizing organisms. *Annu. Rev. Earth Planet. Sci.* 40, 221–249.
- Salio, P., Nicolini, M., Saulo, A.C., 2002. Chaco low-level jet events characterization during the austral summer season. *J. Geophys. Res.* 107 (D24), 4816.
- Saulo, A.C., Seluchi, M.E., Nicolini, B., Aires, B., Previsa, C.D., Paulista, C., 2004. A case study of a Chaco low-level jet event. *Mon. Weather Rev.* 132 (11), 2669–2683.
- Schemmel, F., Mikes, T., Rojay, B., Mulch, A., 2013. The impact of topography on isotopes in precipitation across the Central Anatolian Plateau (Turkey). *Am. J. Sci.* 313 (2), 61–80.
- Sobel, E.R., Strecker, M.R., 2003. Uplift, exhumation and precipitation: tectonic and climatic control of Late Cenozoic landscape evolution in the northern Sierras Pampeanas, Argentina. *Basin Res.* 15 (4), 431–451.
- Stewart, M., 1975. Stable isotope fractionation due to evaporation and isotopic exchange of falling waterdrops: applications to atmospheric processes and evaporation of lakes. *J. Geophys. Res.* 80 (9), 1133–1146.
- Strecker, M.R., Cerveny, P., Bloom, A.L., Malizia, D., 1989. Late Cenozoic tectonism and landscape development in the foreland of the Andes: Northern Sierras Pampeanas (26–28° S), Argentina. *Tectonics* 8 (3), 517–534.
- Uba, C.E., Strecker, M.R., Schmitt, A.K., 2007. Increased sediment accumulation rates and climatic forcing in the central Andes during the late Miocene. *Geology* 35 (11), 979–982. <http://dx.doi.org/10.1130/G224025A1>.
- Vera, C., et al., 2006. Toward a unified view of the American monsoon systems. *J. Climate* 19 (20), 4977–5000.
- Vuille, M., Bradley, R.S., Werner, M., Keimig, F., 2003. 20th century climate change in the tropical Andes: observation and model results. *Adv. Glob. Change Res.* 15, 75–99.
- Wan, Z., 2008. New refinements and validation of the MODIS land-surface Temperature/Emissivity products. *Remote Sens. Environ.* 112 (1), 59–74.
- Wan, Z., Zhang, Y., Zhang, Q., Li, Z., 2002. Validation of the land-surface temperature products retrieved from Terra Moderate Resolution Imaging Spectroradiometer data. *Remote Sens. Environ.* 83 (1–2), 163–180.
- Worden, J., Noone, D., Bowman, K., 2007. Importance of rain evaporation and continental convection in the tropical water cycle. *Nature* 445 (7127), 528–532.
- Zipser, E.J., Liu, C., Cecil, D.J., Nesbitt, S.W., Yorty, D.P., 2006. Where are the most intense thunderstorms on Earth? *Bull. Am. Meteorol. Soc.* 87 (8), 1057–1071.